# Low/Intermediate Temperature Pyrolyzed Polysiloxane Derived Ceramics with Increased Carbon for Electrical Applications

Michelle Greenough<sup>a</sup>, Zeyu Zhao<sup>a</sup>, Luiz G. Jacobsohn<sup>a</sup>, Jianhua Tong<sup>a</sup>, Rajendra K.

Bordia<sup>a</sup>

<sup>a</sup> Materials Science and Engineering Department, Clemson University, Clemson, SC **Abstract** 

This study focuses on the chemistry, thermal stability, and electrical conductivity of low/intermediate pyrolysis temperature (700-900 °C) polysiloxane derived ceramics. These ceramics were modified with additional carbon derived from divinylbenzene (DVB) added to the precursor. Their electrical properties were investigated for potential uses in micro-electrical mechanical systems (MEMS) and anodes for lithium batteries. The microstructure and chemical composition was investigated by attenuated total reflectance Fourier transform infrared spectroscopy (ATR-FTIR), Raman spectroscopy, and x-ray photoelectron spectroscopy (XPS); thermogravimetric analysis (TGA) provided insight into the thermal stability; and electrochemical impedance spectroscopy (EIS) into the electrical properties of the material. The increase of pyrolysis temperature and carbon content lead to an enhancement of the electrical conductivity, higher than previously reported values for intermediate pyrolysis temperature SiOC polymer derived ceramics. A limit of the amount of DVB that can be added to PHMS to produce a hybrid precursor has also been obtained.

## **Keywords**

Polymer Derived Ceramics, Polysiloxane, Hybrid Precursor, Raman Spectroscopy, Electrical Conductivity

#### 1. Introduction

Polymer Derived Ceramics (PDCs) are an important class of ceramics being widely investigated because their compositions can be molecularly tailored over a broad range and they can be processed using conventional polymer processing routes. These attributes lead to the ability to make a wide composition of materials and material forms [1-3]. The majority of these materials are from silicon-based polymers such as polycarbosilanes, polysilazanes, and polysiloxanes [2]. Polysiloxanes have a high ceramic yield because of the high crosslinking density in the precursor [4]. The polymer precursor, heating rate, pyrolysis temperature and atmosphere have a significant effect on the resultant ceramic materials and their properties. Polysiloxanes are of significant interest because the ceramics derived from them are stable up to 1500 °C resulting in high mechanical and chemical stability [4]. Another advantage of polysiloxane derived ceramics is that the crosslinking of this polymer can be done at relatively low temperatures (100-400 °C) [4], which can be further lowered to room temperature by using crosslinking agents [5,6]. Pyrolysis of polysiloxanes has been done typically in the temperature range of 800 – 1500 °C resulting in materials with high thermomechanical and chemical stability, especially for materials pyrolyzed above 1000 °C [4,7–9]. PDC coatings made from particle filled polysiloxanes have been shown to provide excellent protection in highly corrosive and oxidizing environments [10– 12]. Finally, polysiloxane derived PDCs pyrolyzed at temperatures above 800 °C have been shown to be semi-conductor materials. It has been shown that increasing pyrolysis temperature increases electrical conductivity [13].

The addition of other chemical elements to the polymer network allows for improvement and tailorability of key characteristics [5,14]. For example, adding excess carbon, for instance by adding carbon precursors such as divinyl benzene (DVB), to polycarbosilanes leads to significant increase in the electrical conductivity for potential use in micro electrical mechanical systems (MEMS) [15]. Incorporating DVB into the system results in the formation of a "free carbon" phase [5,9], which can be used for tailoring the electrical properties of the resultant PDC [16–20]. The mechanical properties of polysiloxane derived PDC with excess carbon have also been evaluated and it has been shown that both the elastic modulus and the hardness decreases as the excess carbon increases [21]. The use of a liner polymer such as polymethylhydrosiloxane (PHMS) compared to a cyclic one helped to improve the chemical stability, when incorporating DVB [22]. Finally, the incorporation of graphene and graphene oxides in polysiloxanes to increase electrical conductivity has also been investigated [23,24].

Although PDCs obtained at pyrolysis temperature higher than 1000 °C have been widely investigated, limited research has been reported on materials processed by pyrolyzing polysiloxanes at intermediate temperature (within 700-1000 °C). Materials formed by pyrolysis at the lower end of this temperature have been called "ceramers" [25], and it has been shown that these materials have high surface area, tailorable porosity and the ability to incorporate different catalytic elements such as platinum and zinc [25–28]. Although amorphous, these materials retain many desired properties of PDCs including mechanical, chemical, and thermal stability.

The overall goal of this study is to investigate the effect of pyrolysis temperature, in the intermediate temperature range (700 °C to 900 °C), on the chemical and structural changes in polysiloxane derived ceramics with excess carbon introduced using hybridization of PHMS with

DVB. The effect of excess carbon and pyrolysis temperature on the electrical conductivity was also investigated and correlated with the structural and chemical changes.

# 2. Experimental Procedure

### 2.1 Materials and Processing

Commercially available polymethylhydrosiloxane (PHMS) (98-100%, MW: 2100-2400, Gelest, Morrisville, PA) and divinylbenzene (DVB) (technical grade 80%, Sigma Aldrich, St. Louis, MO) were combined with platinum complex (platinum divinyltetramethyldisiloxane 2% in xylene) (Gelest, Morrisville, PA) that was diluted to 0.1% in xylene (Semiconductor grade, Alfa Aesar, Ward Hill, MA). 40µl of Pt complex was used as a crosslinking agent per 1g of PHMS. The research was conducted on a series of samples in which the weight ratio of DVB to PHMS was varied from 0 to 6. The crosslinked samples are labeled as: dvbn (n referring to the ratio of DVB: PHMS (weight ratio). For the pyrolyzed samples, the pyrolysis temperature was added to the sample designation (Table I).

Sample designation for crosslinked samples	
dvbn (n=0 to 6)	
Sample designation for pyrolyzed samples	
700C dvbn, 800C dvbn, or 900C dvbn (n=0 to 6)	

**Table I.** Designation of crosslinked and pyrolyzed samples.

PHMS, DVB and Pt complex were stirred for two minutes and thin (approximately 0.5 mm thickness) polymer films were cast and crosslinked at room temperature. 10 mm diameter disks were cut out of the crosslinked film and pyrolyzed in ultrahigh purity argon (Airgas, Radnor, PA) with 1 °C/min heating rate to the isothermal temperature followed by a two-hour hold at the desired temperature (700, 800 and 900 °C) and a 1 °C/min cooling rate (in an alumina tube in a Lindberg/Blue Furnace).

# 2.2 Characterization and Properties

Thermogravimetric analysis (TGA) was carried out in flowing nitrogen at a heating rate of 10 °C/min up to 1000 °C to determine the mass loss of the samples, as a function of temperature (TGA Q500; TA Instruments, New Castle, DE). Chemical bonding states of the pyrolyzed and crosslinked samples were determined using attenuated total reflectance Fourier transform infrared spectroscopy (ATR FTIR) (Thermo Nicolet Magna 550 FTIR; Thermofisher, Waltham, MA) with a diamond crystal. Samples were manually ground using a mortar and pestle then scanned in 4000 to 525 cm<sup>-1</sup> range. The nature of the carbon-carbon bond was investigated using Raman spectroscopy (Horiba LabRAM HR Evolution Raman; Horiba, Kyoto, Japan). A 532 nm laser source was used at 1% power together with a 600 grooves/mm diffraction grating over a scanning range of 3000 to 500 cm<sup>-1</sup> with a 50x objective lens. The spectra were corrected by the pre-recorded instrument-specific response to a calibrated white light source, namely the intensity correction system (ICS). Peaks were normalized by intensity of the 1600 cm<sup>-1</sup> "G peak". The 1330cm<sup>-1</sup> "D peak" was fit with a Lorentzian function while for the "G peak" a Breit-Wigner-Fano function (BWF) was used consistent with previous research on amorphous carbons [29].

X-ray photoelectron spectroscopy (XPS) measurements were performed to determine the relative abundance of the bonds formed by three key elements: Si, C and O and to investigate the chemical state of these elements. Spectra were obtained using a PHI VersaProbe III Scanning ESCA Microprobe (Physical Electronics Inc, Chanhassen, MN). The PHI VersaProbe III has a monochromatic Al KAl K $\alpha$  X-ray source (hv = 1486.6 eV). The instrument base pressure was maintained better than 1X10<sup>-7</sup> torr. The pyrolyzed samples (approximately 8 mm diameter) were mounted on a stage using nonconductive tape. The XPS beam was at a 45° angle. Carbon (1s) peaks were investigated and deconvoluted to determine binding energies (BE). A survey and high-resolution spectra were run for each sample. Elements responsible for less than 1% of the sample abundance were excluded. For both survey and high-resolution spectra, the Al anode was powered at 25 W and 15 kV. The survey was conducted using three sweeps (0 to 1100 eV), pass energy of 224 eV, dwell time of 50 ms and a step size of 0.8 eV to obtain qualitative elemental analysis. The high-resolution scan was conducted over a narrow energy range around the C(1s)using three sweeps, pass energy of 69 eV and a step size of 0.125 eV. The scans were run over an area of 500 x 500 μm<sup>2</sup> with a 100 μm diameter beam. Charge compensation of samples was accomplished with an electron beam charge neutralization. A sputtering step was used after initial data collection with 2 Kev and 30 s of argon sputtering for the removal of adventitious carbon and oxygen contamination. Peaks position were calibrated to 284.8 eV for carbon for analysis. Data analysis was done using MultiPak (Physical Electronics Inc, Chanhassen, MN) and the elemental peaks were deconvoluted to find the binding energies using CASA XPS software (Casaxps.com, Berlin, Germany) with a Shirley background subtraction while adopting Gaussian-Lorentzian peak shapes (GL(60)), and (FWHM) of 1.2 cm<sup>-1</sup>

For conductivity measurements, silver paste was applied on both sides of the sample (~0.6 mm thickness and ~ 8 mm diameter) by screen printing method and then dried on a hot plate at 150 °C, which worked as current electrodes with attachment of silver mesh and gold leading wires. The electrochemical impedance spectroscopy (EIS) (Gamry Reference 600+) of our pellets was conducted with 10 mV amplitude and frequency a range of 5 MHz to 0.05 Hz under a dry argon atmosphere. The samples were then heated in a Mellen Microtherm Spilt Tube furnace from room temperature to 550 °C with a 5 °C/min heating rate while taking resistance measurements at 50 °C intervals after a 1.5-hour hold time at each temperature point. The EIS results were analyzed by fitting the data with ZView software to obtain the value the intercept of  $Z_{Real}$ -axis in the Nyquist curve which refers to the resistance (R) that was converted into conductivity by the equation of  $\sigma = \frac{l}{R \cdot A}$ , in which l and A refer to the thickness and the area of the pellet, respectively.

## 3. Results

Figure 1 shows the conversion of crosslinked polysiloxane to the pyrolyzed sample at 800 °C.

Crosslinked	Pyrolyzed	Reference
		(3600)
		CEST
10mm	8.3mm	19.75mm

Figure 1. Comparison of SiOC crosslinked and pyrolyzed samples with a reference

Crosslinked samples underwent a shrinkage of approximately 17% after 800 °C pyrolysis. This shrinkage was caused by the loss of organics (as is demonstrated in succeeding sections) in the material and elimination of microporosity.

## 3.1 Attenuated Total Reflectance Fourier Transform Infrared Spectroscopy (FTIR)

ATR FTIR was used to characterize the effects of addition of DVB and pyrolysis conditions on the chemical bonding, specifically the crosslinking of the samples. Previously, FTIR has been used to gain insight into the crosslinking mechanism of polysiloxane with DVB and the effect of pyrolysis temperature [22]. We expect that the crosslinking mechanism will be the same as previously determined and for the pyrolyzed samples the number and intensity of organic bonds (i.e. C-C, C-H) will decrease [22].

Crosslinked sample with divinyl benzene shows, as seen in Figure 2, several distinct chemical bonds: C-H<sub>n</sub> bonds in the 2960-2870cm<sup>-1</sup> range, Si-H stretching bond at 2160cm<sup>-1</sup>, (Si-H<sub>2</sub>)<sub>n</sub> wagging and bend-scissors modes at 843 and 890 cm<sup>-1</sup>, respectively, Si-CH<sub>3</sub> stretching bond at 1260cm<sup>-1</sup> and rocking at 760cm<sup>-1</sup>, Si-CH<sub>2</sub>-Si bond at 1180cm<sup>-1</sup>, Si-O bonds at 1030cm<sup>-1</sup> and 1080cm<sup>-1</sup>, and C-C bonds in the 1400-1625cm<sup>-1</sup> range [22].

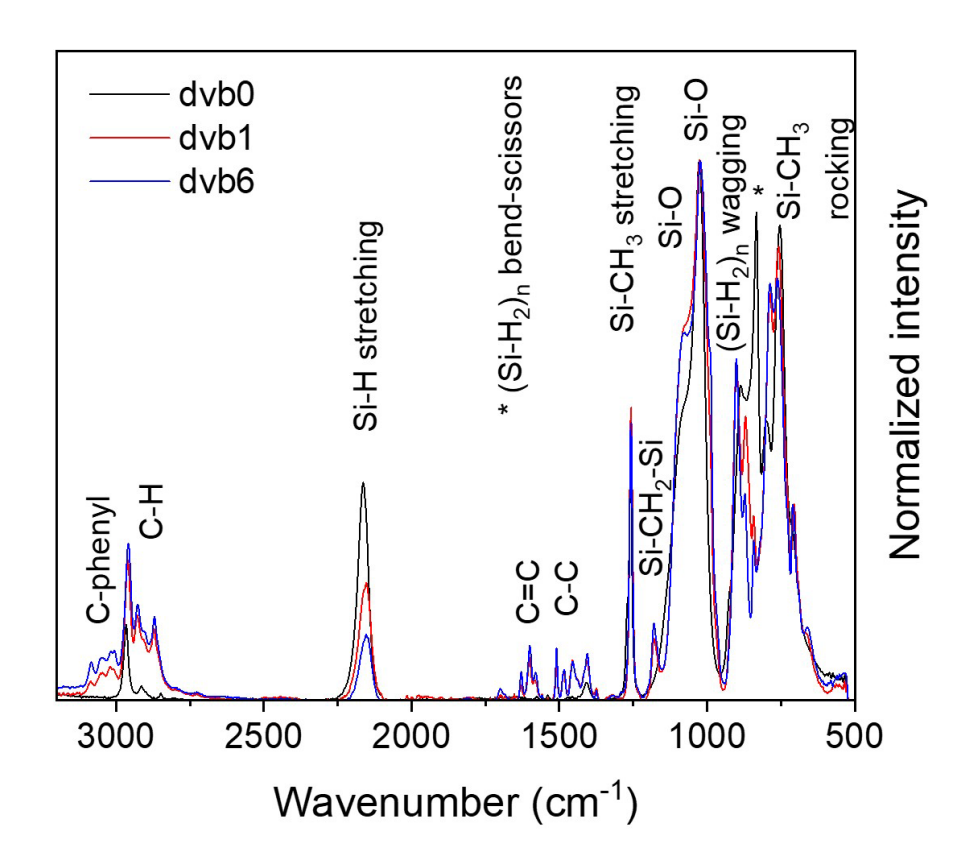


Figure 2. ATR FTIR spectra of crosslinked dvb 0, 1 and 6 samples at room temperature.

The FTIR spectra of samples crosslinked, at room temperature, with and without DVB are compared in Figure 2 for representative *n* values. The lack of DVB is associated with absence of 1180cm<sup>-1</sup> peak for Si-CH<sub>2</sub>-Si and 1400 to 1625cm<sup>-1</sup> bands for C-C and C=C bonding. When DVB is present, a hydrosilylation reaction takes place forming Si-CH<sub>2</sub>-Si bonds instead of unsaturated carbon creating a crosslinked network, as previously reported in literature [22]. This role of DVB in crosslinking of PHMS leads to a hybrid PHMS-DVB precursor. As the amount of DVB:PHMS (*n*) is increased from n= 1 to n=6, there is a relative decrease of the Si-H peak at 2160cm<sup>-1</sup>, of the (Si-H<sub>2</sub>)<sub>n</sub> bend-scissors peak at ~840 cm<sup>-1</sup> and of the 760cm<sup>-1</sup> of SiCH<sub>3</sub> rocking

concomitant to an enhancement of the C-C and C=C bonds around 1500 cm<sup>-1</sup>, Si-CH<sub>2</sub>-Si bonds at 1180cm<sup>-1</sup>, Si-O peak at 1083 cm<sup>-1</sup>, and C-H region at 3000cm<sup>-1</sup>. These observations illustrate that overall, the incorporation of DVB leads to Si oxidation, a decrease of terminal groups bonded to Si and the formation of carbon-based network.

The changes in the chemical bonding were also investigated after pyrolysis at 800 °C. Only Si-O-Si and Si-C bonds could be detected as shown in Figure 3. The chemical bonding changes have been correlated with the TGA results discussed in section 4.

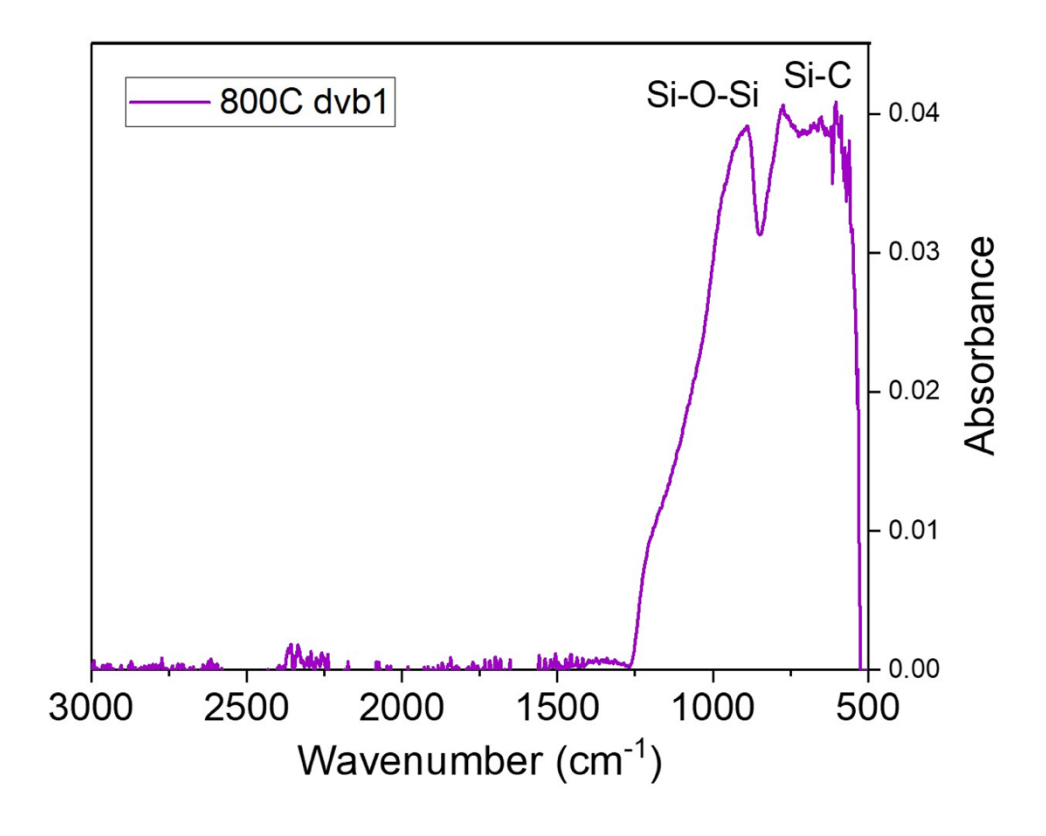
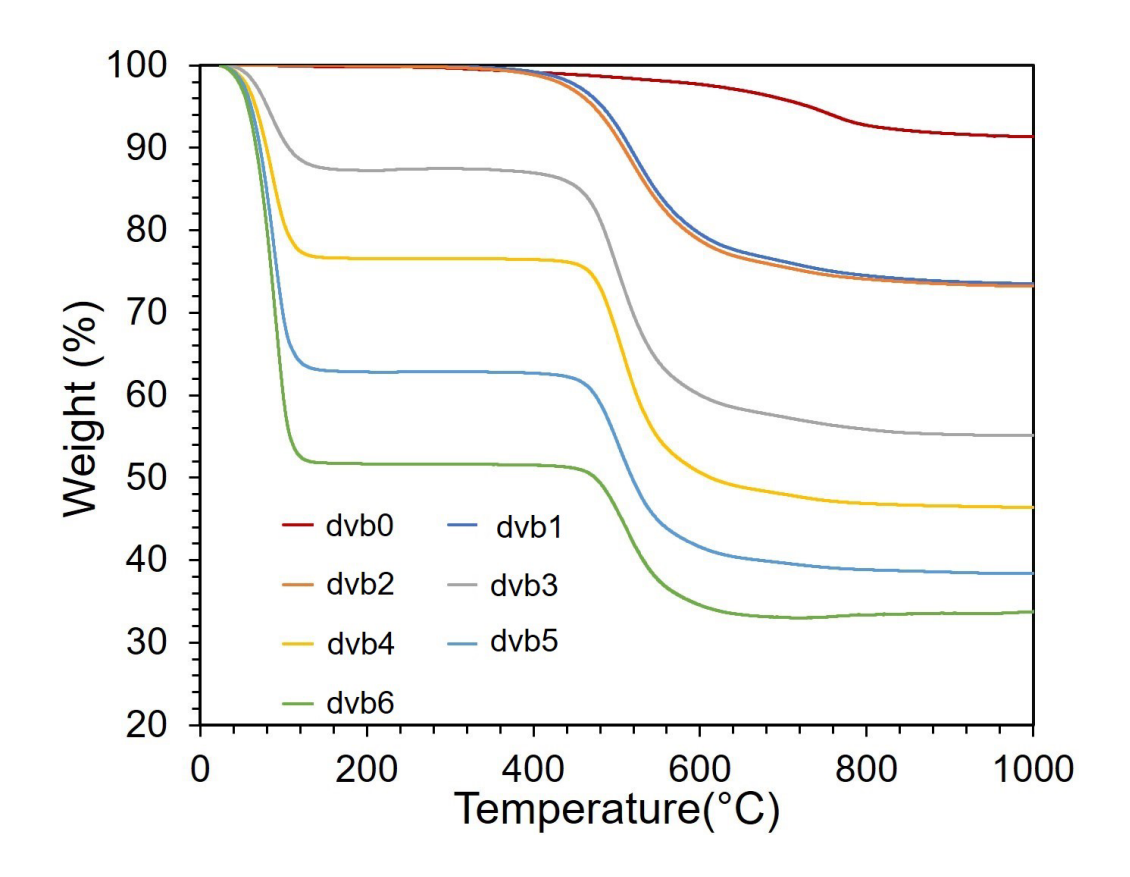


Figure 3. FTIR spectrum of dvb1 sample pyrolyzed at 800 °C

# 3.2 Thermogravimetric Analysis (TGA)

TGA, in inert environment, was used to investigate the effect of DVB:PHMS ratio (n) on the thermal stability and the ceramic yield of the crosslinked samples. The samples were heat treated in nitrogen atmosphere with a heating rate of 10 °C/minute. Thermal stability of the samples was determined by comparing the ceramic yields and decomposition temperature. As shown in Figure 4, for all samples with n > 2, there are two regions of weight loss.



**Figure 4.** Weight loss as a function of temperature of crosslinked samples dvbn; n=0,1,2,3,4,5 and 6.

This is confirmed by Figure 5 in which the derivative of the weight loss is plotted as a function of temperature. The first region of interest between 50-150 °C where initial weight loss occurs due to the loss of hydrogen and water [30]. It is clear that as the amount of DVB increases

beyond 200 % of PHMS, the weight loss in this range is significant. In the range of 400 °C to 600 °C, the weight loss corresponded to the loss of incorporated hydrocarbons. After 600 °C, the samples stabilize and there is no further weight loss. Table II demonstrates that the dvb1 and dvb2 samples show minimal weight loss in region one, showing that all the DVB is being incorporated into the precursor material. For higher levels of DVB, starting from dvb3 there is a significant weight loss in region one showing that not all the DVB is incorporated into the siloxane precursor possibly due to the steric hinderance of DVB and limited crosslinking sites. In addition, for n > 3, the low temperature weight loss increases as the amount of DVB increases indicating that the free DVB contributes to incorporation of water, from environment, and this water is lost in the low temperature regime. This is likely due to the fact that the crosslinked samples were exposed to lab air for a period of time between 24 to 48 hours before the TGA analysis was conducted. It was shown in Ref. 30 that aging of the samples increases the weight loss in the low temperature regime due to water from environment.

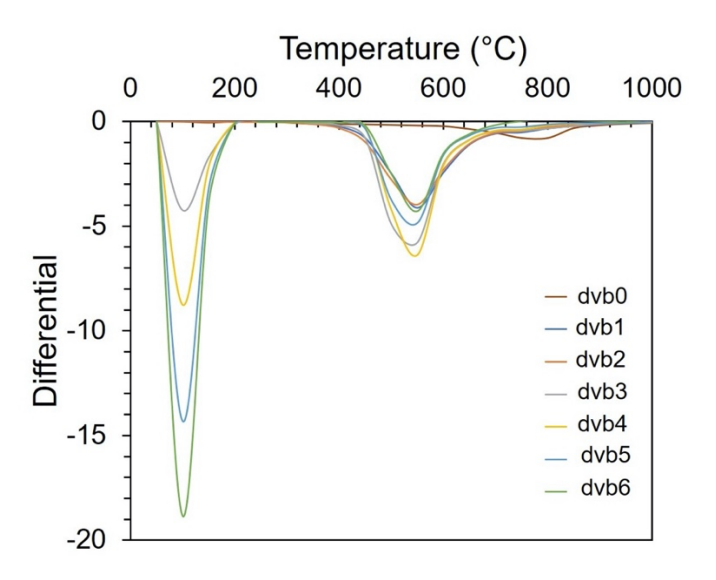


*Figure 5.* Derivative of the weight loss of crosslinked samples dvbn; n=0,1,2,3,4,5 and 6.

	Weight loss region 1	Weight loss region 2
Temperature range	50-150 (°C)	400-600 (°C)
dvb1	0.01	19.65
dvb2	0.01	20.08
dvb3	11.89	26.94
dvb4	21.75	25.83
dvb5	34.95	21.07
dvb6	45.4	16.98

**Table II.** From TGA data, percent weight loss in weight loss region 1 (50 to 150 °C) and weight loss region 2 (400-600 °C) for crosslinked samples-dvbn; n=1 to 6

This trend can further be illustrated by plotting the weight loss in the two regions as a function of DVB (Figure 6). The weight loss in region 1 increases linearly as the DVB content increases beyond dvb3. The higher temperature weight loss has no clear dependence on the DVB content, and it is in the range of 20 to 25 % for all samples

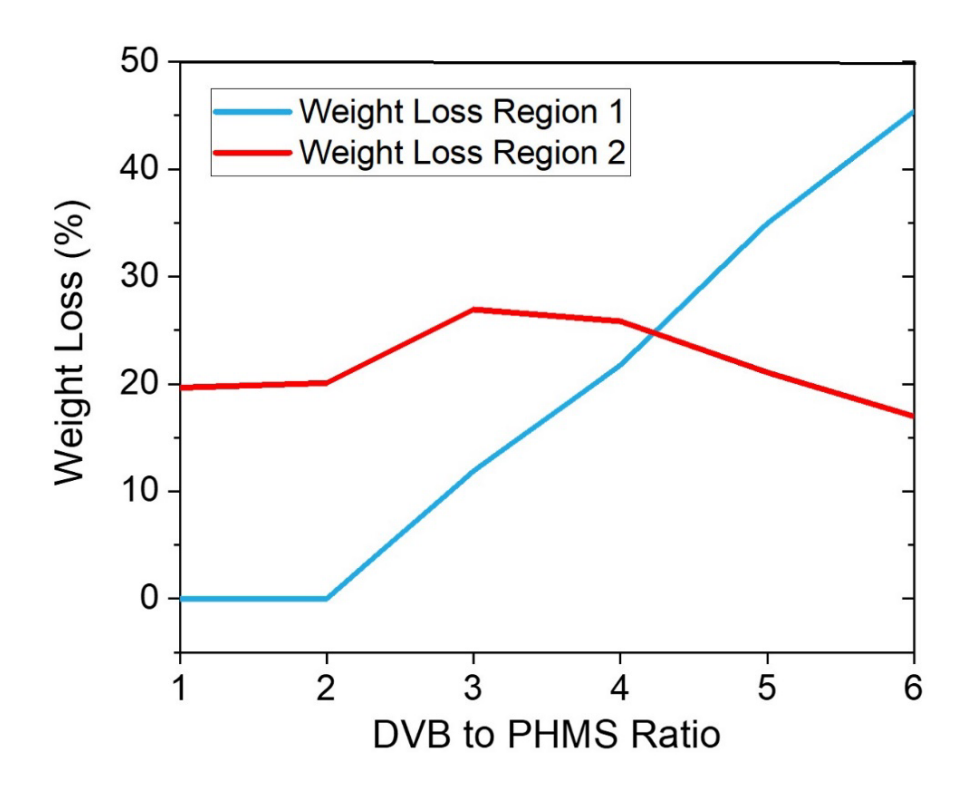


**Figure 6.** Percent weight loss vs amount of DVB from TGA of crosslinked samples for weight loss region 1 (50 to 150 °C) and weight loss region 2 (400 to 600 °C).

The TGA results clearly shows that up to a DVB:PHMS ratio of 2, the DVB becomes part of the hybrid precursor and beyond that DVB remains unreacted.

## 3.3 Raman Spectroscopy

Raman spectroscopy of carbon based materials presents two major bands, the G-band, centered around  $1570 \text{ cm}^{-1}$ , that is associated with the optically allowed  $E_{2g}$  zone center of crystalline graphite, and the D-band, at around  $1400 \text{ cm}^{-1}$ , associated with disorder-allowed zone edge modes of graphite that becomes Raman active due to the lack of long-range order [31]. The effect of the pyrolysis temperatures and carbon content on the D and G bands of amorphous

carbon materials has been investigated [29,32]. In this work, Raman spectroscopy was used to characterize the effects of the pyrolysis temperature on the carbon-carbon bonding through the analysis of the D and G bands. Figure 7 illustrates the effects of different pyrolysis temperatures on the Raman spectra, normalized to by the intensity of the G peak at 1603cm<sup>-1</sup>. The peak position, full width at half maximum (FWHM), and peak intensity ratio I(D)/I(G) (determined in terms of area (A) and height (H)) were extracted by spectral fitting as illustrated in Fig. 8 for dvb1. Fitting results are presented in Table III. As the pyrolysis temperature increases, the I(D)/I(G) ratio increases in both area and height. The position of the D and G peaks remain in a similar range of 1328 to 1333cm<sup>-1</sup> and 1606 to 1608cm<sup>-1</sup>, respectively. The D band narrowing together with the increase of the I(D)/I(G) ratio for higher pyrolysis temperatures indicate an increase in the size and/or number of the ordered graphitic domains [29].

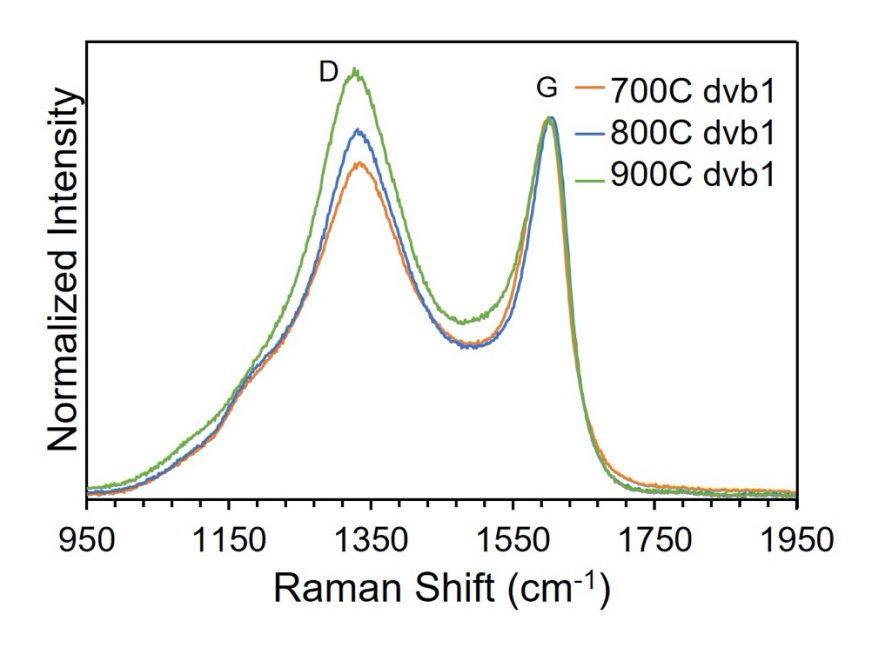
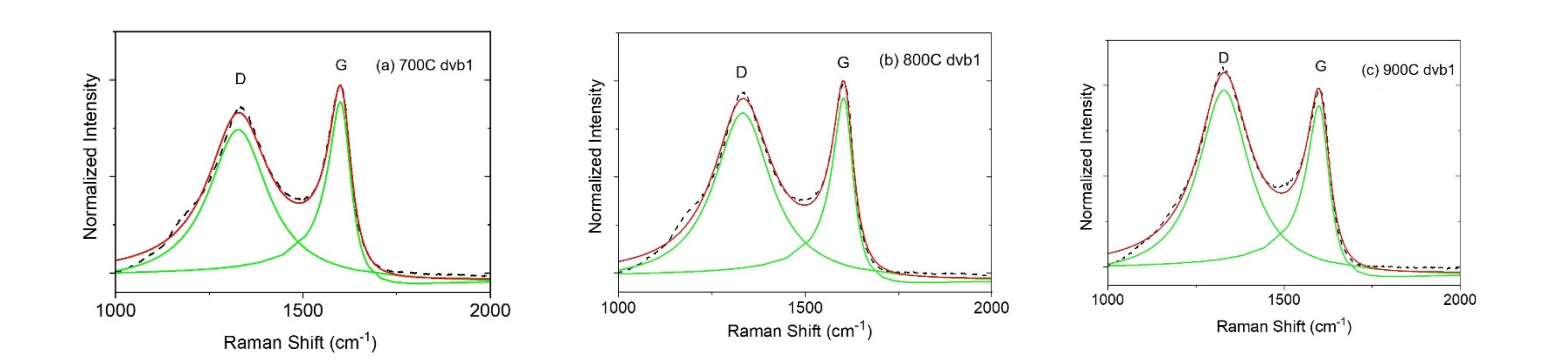


Figure 7. Raman of dvb1 pyrolyzed at temperatures of 700,800 and 900 °C.

Sample	Position D	FWHM	Position G	FWHM	I(D)/I(G) A	I(D)/I(G) H
	(cm <sup>-1</sup> )	(cm <sup>-1</sup> )	(cm <sup>-1</sup> )	(cm <sup>-1</sup> )		
700C dvb1	1328	194	1607	78	1.6	0.84
800C dvb1	1333	187	1608	71	1.8	0.92
900C dvb1	1329	176	1606	83	1.8	1.1

**Table III.** Results of Raman analysis in terms of D and G bands peak position, full width at half max (FWHM) and I(D)/I(G) ratio based on area (A) and height (H) of sample dvb1 pyrolyzed at  $700 \, ^{\circ}C$ ,  $800 \, ^{\circ}C$  and  $900 \, ^{\circ}C$ .



**Figure 8.** Raman spectra with best fits of dvb1 pyrolyzed at: (a) 700 °C, (b) 800 °C, and (c) 900 °C.

The comparison of samples with different of amounts of DVB pyrolyzed at 800 °C is presented in Figure 9, where spectra were normalized to the G peak maximum. The peak position, FWHM, and I(D)/I(G) ratios are reported in Table IV for samples with different amounts of DVB

pyrolyzed at 800 °C. As DVB increased, there is no major change of the I(D)/I(G) ratio as can be inferred from Figure 9 and Table IV. The increase of I(D)/I(G) ratio has been associated with the increase in size and/or number of the  $sp^2$  domains [33]. The lack of observed change of the I(D)/I(G) ratio indicated that there was no substantial change in the structure of carbon in these materials.

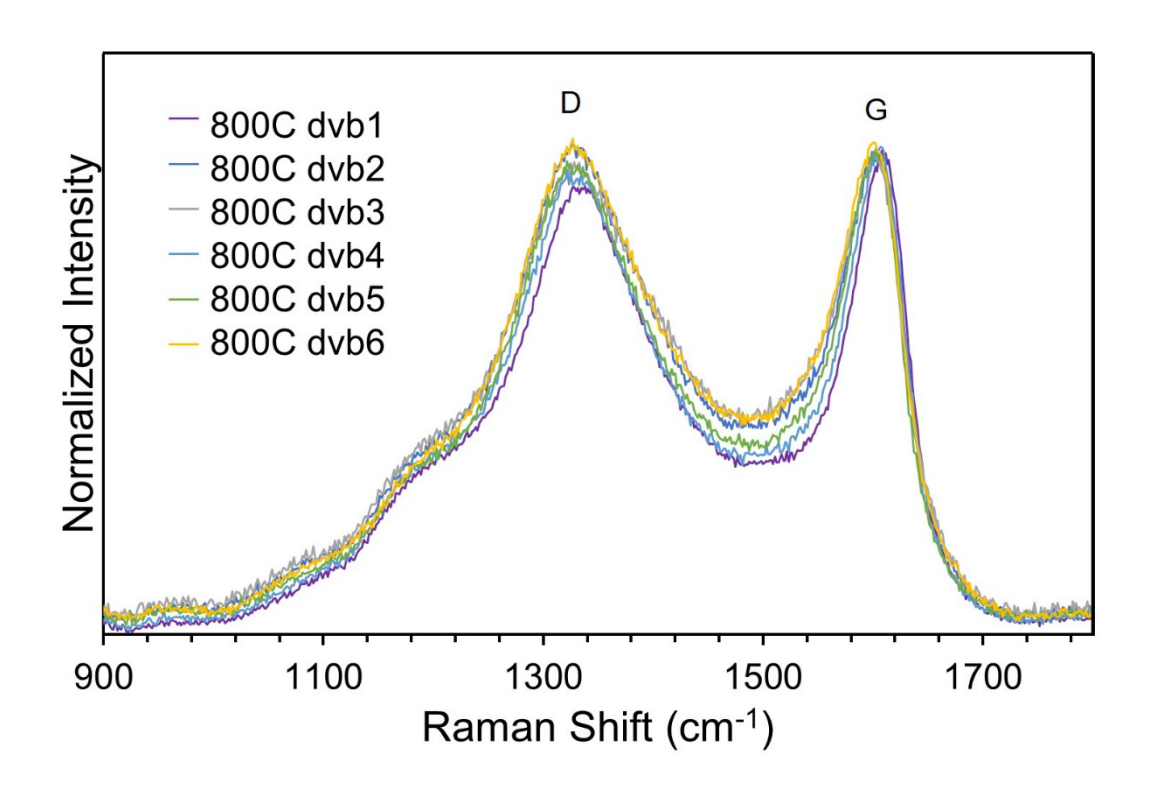


*Figure 9.* Raman of dvbn for n from 1 to 6 for all pyrolyzed at 800 °C.

Sample	Position D	FWHM	Position G	FWHM	I(D)/I(G) A	I(D)/I(G) H
	(cm <sup>-1</sup> )	(cm <sup>-1</sup> )	(cm <sup>-1</sup> )	(cm <sup>-1</sup> )		
800C dvb1	1333	187	1608	71	1.8	0.92

800C dvb2	1334	220	1597	70	3.1	1.1
800C dvb3	1328	248	1605	72	3.4	1.1
800C dvb4	1328	219	1605	62	3.1	0.98
800C dvb5	1323	218	1602	67	3.0	1.0
800C dvb6	1325	228	1602	74	3.0	1.1

**Table IV.** Raman values of peak position for D and G, full width at half max (FWHM) and I(D)/I(G) ratio for area (A) and heigh (H) of dvbn samples pyrolyzed at 800 °C (n from 1 to 6).

# 3.4 X-Ray photoelectron spectroscopy (XPS)

XPS was used to determine the chemical bonding of C in selected samples (800C dvb1, 800C dvb6, 700C dvb1 and 900C dvb1). This was done by comparing binding energies (BE) and percent abundance within the C (*Is*) spectrum. Figure 10 a-d shows C (*Is*) bonding that includes Si-C, Si-O-C, C=C (sp²), C-C/H (sp³) and C-O bonds. Their binding energies are identified in Table V based on literature values [34–36]. The effect of increase in carbon (*i.e.*, higher DVB content) and pyrolysis temperature were analyzed in terms of C-Si, C-Si-O, C=C, C-C/H and C-O bonding relative intensities shown as peaks in Figure 10.

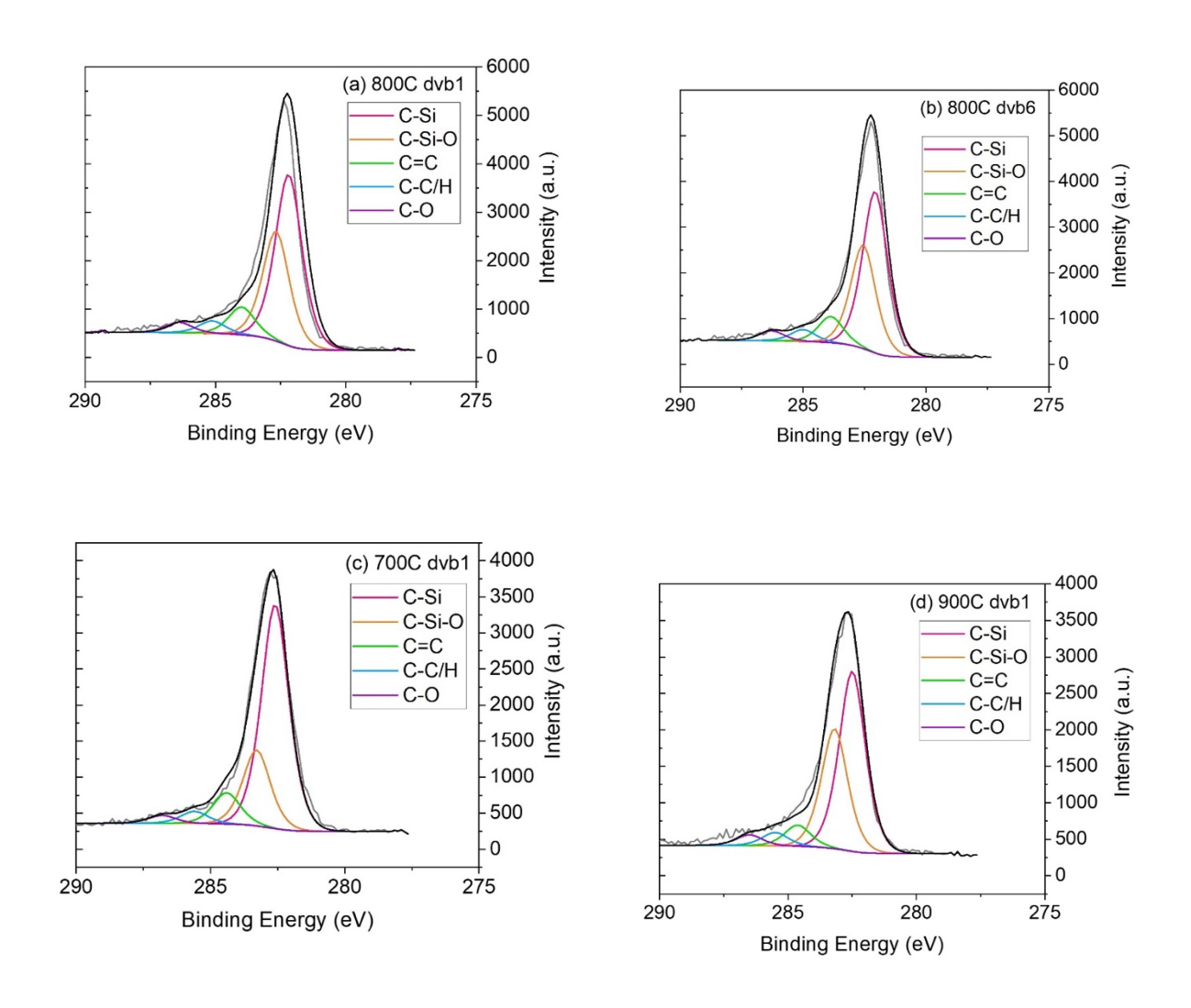


**Figure 10.** XPS spectra of C 1s (a) 800C dvb1, (b) 800C dvb6, (c) 700C dvb1 and (d) 900C dvb1.

	C-Si BE (eV)	C-Si-O BE (eV)	C=C BE (eV)	C-C/H BE (eV)	C-O BE (eV)
700C dvb1	282.6	283.3	284.4	285.6	286.8

800C dvb1	282.0	282.8	284.0	285.0	285.9
900C dvb1	282.5	283.2	284.6	285.5	286.5
800C dvb6	282.1	282.6	283.9	285.0	286.3

**Table V.** XPS binding energies (BE) of C1s for samples 800C dvb1, 800C dvb6, 700C dvb1 and 900C dvb1.

Using XPS results, Table VI summarizes the chemical bond presence in terms of abundance percent for the samples investigated. These results are discussed in the discussion section.

	C-Si	C-Si-O	C=C	С-С/Н	C-O
	(%)	(%)	(%)	(%)	(%)
700C dvb1	64	22	9	3	2
800C dvb1	63	27	6	2	2
900C dvb1	52	35	6	4	3
800C dvb6	52	33	8	4	3

**Table VI.** Summary of the analysis of XPS high resolution scans of C 1s. Each scan set of results add up to 100%.

The XPS results show the changes in the abundance of various chemical bonds both as a function of the DVB content in the precursor and the pyrolysis temperature. Specifically, for the same pyrolysis temperature (800 °C), as the DVB content increases (from n = 1 to n = 6), the most

significant change is in the decrease of the abundance of the C-Si bonds and an increase in the abundance of the C-Si-O bonds. The other C containing bonds become slightly more abundant. For the same DVB content (n=1), as the pyrolysis temperature increases, the abundance of the C-Si bond decreases, the C-Si-O bond increases and the C=C decreases. These results are further discussed in the discussion section in the context of the conductivity measurements.

## 3.5 Electrical Conductivity

EIS was used to measure the electrical conductivity of the samples. All three samples (800 dvb1, 800 dvb6, and 900 dvb1) exhibited a similar tendency that their conductivity ncreased with increasing temperature from room temperature to 550 °C as seen in Figure 11. In addition, for samples heat treated at the same temperature, 800 °C, samples with higher carbon content had higher conductivity (Figure 11) over the entire temperature range. For example, at 550 °C, the conductivity of dvb6 is around three times higher than that of dvb1. The effect of pyrolysis temperature can also be compared in Figure 11 by comparing dvb1 samples pyrolyzed at 800 °C and 900 °C. For the 900 °C pyrolyzed samples the electrical conductivity is almost thirty times higher, at 500 °C, compared to the sample pyrolyzed at 800 °C. This observation is in agreement with the statement that there is an increase in electrical conductivity as a function of pyrolysis temperature up to 1000 °C, which was reported in a literature [37].

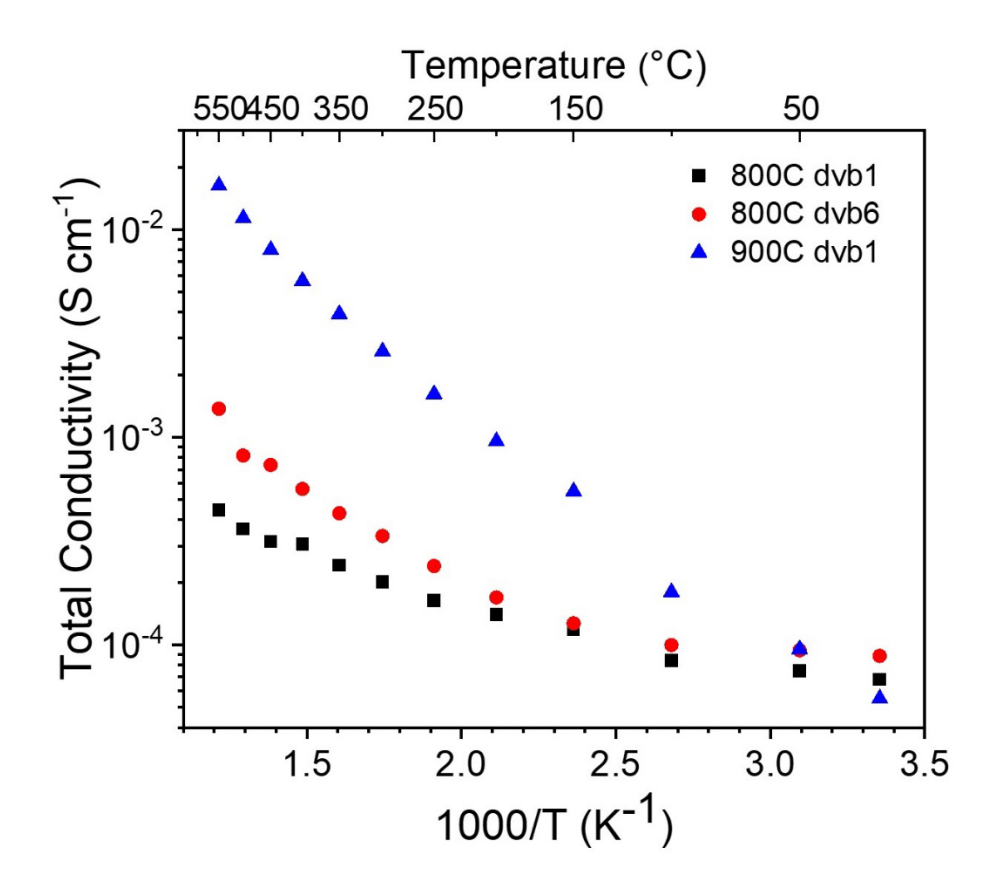


Figure 11. Electrical conductivity as a function of the temperature of sample 800C dvb1, 800C dvb6 and 900C dvb1

## 4. Discussion

Previous research on polysiloxane derived ceramics with carbon additives showed the microstructure to contain continuous amorphous/disordered graphitic and SiOC domains [3]. The graphitic domain is formed from the incorporation of DVB. The amorphous/disordered graphitic domains get more organized and possibly grow in size as pyrolysis temperature increases and is expected to result in an overall conductivity increase. To better understand this phenomena,

detailed chemical investigation by means of ATR FTIR, TGA, Raman, XPS and EIS were conducted. The chemical transformations due to the addition of DVB were evaluated by ATR FTIR with emphasis on the crosslinking. Crosslinked samples containing various percentages of divinyl benzene, for DVB:PHMS weight ratio n from = 0 to 6 were compared to determine the effect of DVB on the chemical bonding in the crosslinked polymer (Figure 2). ATR FTIR results revealed that as the amount of DVB increases, there is a decrease of (Si-H<sub>2</sub>)<sub>n</sub> linear polymeric bonds and Si-CH<sub>3</sub> terminal bonds while Si-CH<sub>2</sub>-Si linear polymeric bonds increased. The elimination of terminal bonds is suggestive of crosslinking. Si-H is consumed during crosslinking with divinylbenzene due to a hydrosilylation reaction, leading to a hybrid precursor. More specifically, Si-H and Si-CH<sub>3</sub> bonds decrease due to DVB substituting for H and CH<sub>3</sub> attached to silicon in the polymer precursor. As the amount of DVB increases, a point is reached such that the increase of DVB in the precursor mixture no longer leads to a proportional increase of the amount of DVB incorporated in the crosslinked polysiloxane. From the results of the mass loss, during heat treatment (Figure 6), it is clear that the relative weight loss is quite different for samples with DVB:PHMS ratio less than or equal to 2 than for higher amounts of DVB. This figure clearly illustrates that for DVB:PHMS greater than 2, the weight loss in the low temperature regime (50 -150 °C) increases proportionately as the amount of DVB increases. These results indicated that a DVB:PHMS weight ratio of 2 is maximum for the being incorporated to create a hybrid DVB-PHMS polymer. Beyond this, a mixture of the two polymers is obtained and the free DVB incorporates low temperature volatile species (most likely water) from the environment.

The incorporation of DVB has been shown to be associated with a more conductive ceramic [15]. This research also shows that as the amount of DVB increases, the electrical conductivity

increases (Figure 11). However, the increase in conductivity is quite small. We found that SiOC ceramics without DVB were insulating and when the ratio of DVB:PHMS was 1 or higher, the samples became semi-conducting. However, a six-fold increase in DVB content only improves the conductivity by a factor of 3 or so (at 550 °C). This result corresponds well with the analysis of free carbon in the study reported in Ref. 21 on polymer derived ceramics from DVB-PHMS. In this study, it was shown that the free carbon increases as the amount of DVB increases. However, the highest increase is for lower amounts of DVB. For example, the free carbon for 1:1 ratio of PHMS:DVB is 30.6 % and is 54.2 for 1:6 ratio. XPS results (Figure 10 and Table V) also show that the difference between the percentage of C=C between samples with DVB:PHMS ratio of 1 and 6 (both heat treated at 800 °C) is small.

The effects of pyrolysis temperature was evaluated as a function of the temperature (Figure 7 and Table III) and carbon content (Figure 9 and Table IV) using Raman spectroscopy. The D band narrowing together with the increase of the I(D)/I(G) ratio for higher pyrolysis temperatures indicated an increase in the size and/or number of the graphitic domains from amorphous carbon [29]. However, when comparing the amount of carbon in the pyrolyzed samples at 800 °C as *n* increased from 1 to 6, no structural changes related to the amorphous carbon/disordered graphitic domains were revealed by Raman spectroscopy. Further insight into the structural evolution was obtained by XPS. Detailed analysis of the carbon binding energy showed that between 800C dvb1 and 800C dvb6, there was a decrease in the amount of C-Si bonding while an increase of the relative abundance of C-Si-O and C=C bonds, as seen in Table VI.

Finally, EIS revealed measurable increase of the electrical conductivity (a factor of 3) due to increasing carbon content. However, the pyrolysis temperature has a major effect. The electrical conductivity, at high temperature increases by almost a factor of thirty when the pyrolysis

temperature is increased from 800 to 900 °C (for same DVB:PHMS ratio). There is a small effect of the increased amount of DVB and this correlates to the increase in small increase in free carbon in going from dvb1 to dvb6 (Table VI). The much larger increase in conductivity as a function of the pyrolysis temperature is explained by the change in the structure of carbon confirmed by Raman by focusing on the I(D)/I(G) ratios (Figures 7 and 8 and Table III).

#### 5. Conclusion

The chemistry, thermal stability and electrical properties of PHMS-DVB blended/hybrid polymers was investigated as a function of stoichiometry and pyrolysis temperature. Thermal stability was determined by TGA, in which, the ceramics retained stability with minimal weight loss above 600 °C. Chemical changes also occurred due to the change in pyrolysis temperature and stoichiometry as seen in FTIR, Raman and XPS. Overall, the increase in pyrolysis temperature showed-an increase in the I(D)/I(G) ratio as seen in Raman. XPS was also able to confirm the presence of carbon bonding (both sp<sup>2</sup> and sp<sup>3</sup>) and carbon-oxygen bonding. The DVB-PHMS hybrid precursor leads to a composite SiOC-C composite. It is shown that the amount of DVB that can be incorporated in the formation of the hybrid polymer, during crosslinking, is limited to around two times the weight of PHMS. Both the increased temperature and carbon content increased the electrical conductivity as a result, an intrinsically insulating SiOC is transformed to a semiconductor due to the addition of free carbon that undergoes a structural change as temperature increases. These results show the promise of being able to make semiconducting SiOC with increased carbon at low processing temperature which are expected to result in high levels of microporosity and surface area. Further investigations are needed to investigate the nature and extent of porosity in these materials. In addition, the nature

of the carbon derived from the hybrid polymer at low temperatures for amorphous ceramics and that from unreacted DVB needs to be investigated.

## Acknowledgements

The authors would like to thank Ms. Kimberly Ivey of Clemson University for her efforts and expertise in FTIR and TGA measurements, Dr. Kelliann Koehler of Clemson EM lab for her XPS expertise. Undergraduate students Olivia Sequerth and Kimberly Garvin are thanked for their assistance with the early stages of preparation and testing of these samples. This work was supported in part by the National Science Foundation EPSCoR Program under NSF Award # OIA-1655740. Addition support from National Science Foundation Graduate Research Fellowship Program GRFP: (DGE-1744593) is also acknowledged. However, opinions, findings and conclusions or recommendations expressed in this material are those of the author(s) and do not necessarily reflect those of the National Science Foundation

#### References

- [1] B. V Manoj Kumar, Y.-W. Kim, Processing of polysiloxane-derived porous ceramics: a review, Sci. Technol. Adv. Mater. (2010). https://doi.org/10.1088/1468-6996/11/6/069801.
- [2] P. Colombo, G. Mera, R. Riedel, G.D. Sorarù, Polymer-derived ceramics: 40 Years of research and innovation in advanced ceramics, J. Am. Ceram. Soc. (2010). https://doi.org/10.1111/j.1551-2916.2010.03876.x.
- [3] Q. Wen, Z. Yu, R. Riedel, The fate and role of in situ formed carbon in polymer-derived ceramics, Prog. Mater. Sci. (2020). https://doi.org/10.1016/j.pmatsci.2019.100623.
- [4] C. Stabler, E. Ionescu, M. Graczyk-Zajac, I. Gonzalo-Juan, R. Riedel, Silicon oxycarbide glasses and glass-ceramics: "All-Rounder" materials for advanced structural and functional applications, J. Am. Ceram. Soc. (2018). https://doi.org/10.1111/jace.15932.
- [5] Y.D. Blum, D.B. MacQueen, H.J. Kleebe, Synthesis and characterization of carbon-enriched silicon oxycarbides, J. Eur. Ceram. Soc. (2005). https://doi.org/10.1016/j.jeurceramsoc.2004.07.019.
- [6] G.D. Sorarù, F. Dalcanale, R. Campostrini, A. Gaston, Y. Blum, S. Carturan, P.R. Aravind, Novel polysiloxane and polycarbosilane aerogels via hydrosilylation of preceramic polymers, J. Mater. Chem. (2012). https://doi.org/10.1039/c2jm00020b.
- [7] R.M. Morcos, A. Navrotsky, T. Varga, Y. Blum, D. Ahn, F. Poli, K. Müller, R. Raj,

- Energetics of SixOyCz polymer-derived ceramics prepared under varying conditions, J. Am. Ceram. Soc. (2008). https://doi.org/10.1111/j.1551-2916.2008.02543.x.
- [8] C. Stabler, A. Reitz, P. Stein, B. Albert, R. Riedel, E. Ionescu, Thermal properties of SiOC glasses and glass ceramics at elevated temperatures, Materials (Basel). (2018). https://doi.org/10.3390/ma11020279.
- [9] G. Mera, A. Navrotsky, S. Sen, H.J. Kleebe, R. Riedel, Polymer-derived SiCN and SiOC ceramics-structure and energetics at the nanoscale, J. Mater. Chem. A. (2013). https://doi.org/10.1039/c2ta00727d.
- [10] G. Barroso, Q. Li, R.K. Bordia, G. Motz, Polymeric and ceramic silicon-based coatings-a review, J. Mater. Chem. A. (2019). https://doi.org/10.1039/c8ta09054h.
- [11] K. Wang, M. Günthner, G. Motz, R.K. Bordia, High performance environmental barrier coatings, Part II: Active filler loaded SiOC system for superalloys, J. Eur. Ceram. Soc. (2011). https://doi.org/10.1016/j.jeurceramsoc.2011.05.047.
- [12] K. Wang, J. Unger, J.D. Torrey, B.D. Flinn, R.K. Bordia, Corrosion resistant polymer derived ceramic composite environmental barrier coatings, J. Eur. Ceram. Soc. (2014). https://doi.org/10.1016/j.jeurceramsoc.2014.05.036.
- [13] J. Cordelair, P. Greil, Electrical conductivity measurements as a microprobe for structure transitions in polysiloxane derived Si-O-C ceramics, J. Eur. Ceram. Soc. (2000). https://doi.org/10.1016/S0955-2219(00)00068-6.
- [14] H.J. Kleebe, Y.D. Blum, SiOC ceramic with high excess free carbon, J. Eur. Ceram. Soc. (2008). https://doi.org/10.1016/j.jeurceramsoc.2007.09.024.
- [15] F. Dalcanale, J. Grossenbacher, G. Blugan, M.R. Gullo, A. Lauria, J. Brugger, H. Tevaearai, T. Graule, M. Niederberger, J. Kuebler, Influence of carbon enrichment on electrical conductivity and processing of polycarbosilane derived ceramic for MEMS applications, J. Eur. Ceram. Soc. (2014). https://doi.org/10.1016/j.jeurceramsoc.2014.06.002.
- [16] G. Liu, J. Kaspar, L.M. Reinold, M. Graczyk-Zajac, R. Riedel, Electrochemical performance of DVB-modified SiOC and SiCN polymer-derived negative electrodes for lithium-ion batteries, Electrochim. Acta. (2013). https://doi.org/10.1016/j.electacta.2013.05.064.
- [17] J. Kaspar, M. Graczyk-Zajac, S. Choudhury, R. Riedel, Impact of the electrical conductivity on the lithium capacity of polymer-derived silicon oxycarbide (SiOC) ceramics, Electrochim. Acta. (2016). https://doi.org/10.1016/j.electacta.2016.08.121.
- [18] M. Graczyk-Zajac, G. Mera, J. Kaspar, R. Riedel, Electrochemical studies of carbon-rich polymer-derived SiCN ceramics as anode materials for lithium-ion batteries, J. Eur. Ceram. Soc. (2010). https://doi.org/10.1016/j.jeurceramsoc.2010.07.010.
- [19] V.S. Pradeep, D.G. Ayana, M. Graczyk-Zajac, G.D. Soraru, R. Riedel, High Rate Capability of SiOC Ceramic Aerogels with Tailored Porosity as Anode Materials for Liion Batteries, Electrochim. Acta. (2015). https://doi.org/10.1016/j.electacta.2015.01.088.
- [20] H. Sun, K. Zhao, Atomistic Origins of High Capacity and High Structural Stability of Polymer-Derived SiOC Anode Materials, ACS Appl. Mater. Interfaces. (2017). https://doi.org/10.1021/acsami.7b10906.
- [21] G.D. Sorarù, L. Kundanati, B. Santhosh, N. Pugno, Influence of free carbon on the Young's modulus and hardness of polymer-derived silicon oxycarbide glasses, J. Am. Ceram. Soc. (2019). https://doi.org/10.1111/jace.16131.
- [22] P. Dibandjo, S. Diré, F. Babonneau, G.D. Soraru, Influence of the polymer architecture on

- the high temperature behavior of SiCO glasses: A comparison between linear- and cyclic-derived precursors, J. Non. Cryst. Solids. (2010). https://doi.org/10.1016/j.jnoncrysol.2009.10.006.
- [23] C. Shen, E. Barrios, L. Zhai, Bulk Polymer-Derived Ceramic Composites of Graphene Oxide, ACS Omega. (2018). https://doi.org/10.1021/acsomega.8b00492.
- [24] R. Sujith, P.K. Chauhan, J. Gangadhar, A. Maheshwari, Graphene nanoplatelets as nanofillers in mesoporous silicon oxycarbide polymer derived ceramics, Sci. Rep. (2018). https://doi.org/10.1038/s41598-018-36080-1.
- [25] M. Wilhelm, C. Soltmann, D. Koch, G. Grathwohl, Ceramers Functional materials for adsorption techniques, J. Eur. Ceram. Soc. 25 (2005) 271–276. https://doi.org/10.1016/j.jeurceramsoc.2004.08.008.
- [26] M. Adam, M. Bäumer, M. Schowalter, J. Birkenstock, M. Wilhelm, G. Grathwohl, Generation of Pt- and Pt/Zn-containing ceramers and their structuring as macro/microporous foams, Chem. Eng. J. (2014). https://doi.org/10.1016/j.cej.2014.02.063.
- [27] M. Adam, S. Kocanis, T. Fey, M. Wilhelm, G. Grathwohl, Hierarchically ordered foams derived from polysiloxanes with catalytically active coatings, J. Eur. Ceram. Soc. (2014). https://doi.org/10.1016/j.jeurceramsoc.2013.12.011.
- [28] M. Adam, M. Wilhelm, G. Grathwohl, Polysiloxane derived hybrid ceramics with nanodispersed Pt, Microporous Mesoporous Mater. (2012). https://doi.org/10.1016/j.micromeso.2011.10.037.
- [29] A. Ferrari, J. Robertson, Interpretation of Raman spectra of disordered and amorphous carbon, Phys. Rev. B Condens. Matter Mater. Phys. (2000). https://doi.org/10.1103/PhysRevB.61.14095.
- [30] D. Hourlier, S. Venkatachalam, M.R. Ammar, Y. Blum, Pyrolytic conversion of organopolysiloxanes, J. Anal. Appl. Pyrolysis. (2017). https://doi.org/10.1016/j.jaap.2016.11.016.
- [31] TUINSTRA F, KOENIG JL, RAMAN SPECTRUM OF GRAPHITE, J. Chem. Phys. (1970). https://doi.org/10.1063/1.1674108.
- [32] L.G. Jacobsohn, R. Prioli, F.L. Freire, G. Mariotto, M.M. Lacerda, Y.W. Chung, Comparative study of anneal-induced modifications of amorphous carbon films deposited by dc magnetron sputtering at different argon plasma pressures, in: Diam. Relat. Mater., 2000. https://doi.org/10.1016/S0925-9635(99)00341-6.
- [33] R.O. Dillon, J.A. Woollam, V. Katkanant, Use of Raman scattering to investigate disorder and crystallite formation in as-deposited and annealed carbon films, Phys. Rev. B. (1984). https://doi.org/10.1103/PhysRevB.29.3482.
- [34] M.D. Irwin, C.G. Pantano, P. Gluche, E. Kohn, Bias-enhanced nucleation of diamond on silicon dioxide, Appl. Phys. Lett. (1997). https://doi.org/10.1063/1.119839.
- [35] A.S. Rudenkov, A. V. Rogachev, A.N. Kupo, P.A. Luchnikov, N. Chicherina, The phase composition and structure of silicon-carbon coatings, Mater. Sci. Forum. (2019). https://doi.org/10.4028/www.scientific.net/MSF.970.283.
- [36] K. Wang, B. Ma, X. Li, Y. Wang, L. An, Structural evolutions in polymer-derived carbon-rich amorphous silicon carbide, J. Phys. Chem. A. (2015). https://doi.org/10.1021/jp5093916.
- [37] K. Lu, Porous and high surface area silicon oxycarbide-based materials A review, Mater. Sci. Eng. R Reports. (2015). https://doi.org/10.1016/j.mser.2015.09.001.